Peptides 119 (2019) 170119

Contents lists available at ScienceDirect

Peptides

journal homepage: www.elsevier.com/locate/peptides

Understanding interactions of Citropin 1.1 analogues with model membranes and their influence on biological activity

Nathalia Rodrigues de Almeida[a,1], Jonathan Catazaro[b,1], Maddeboina Krishnaiah[c], Yashpal Singh Chhonker[d], Daryl J. Murry[d], Robert Powers[b,e,*], Martin Conda-Sheridan[a,**]

[a] Department of Pharmaceutical Sciences, University of Nebraska Medical Center – Omaha, NE, 68198-6125, USA
[b] Department of Chemistry, University of Nebraska – Lincoln, NE, 68588-0304, USA
[c] Department of Pediatrics Computational Chemistry, University of Nebraska Medical Center – Omaha, NE, 68198-2168, USA
[d] Clinical Pharmacology Laboratory, Department of Pharmacy Practice, University of Nebraska Medical Center – Omaha, NE, 68198-6145, USA
[e] Nebraska Center for Integrated Biomolecular Communication, Lincoln, NE, 68588-0304, USA

ARTICLE INFO

Keywords:
Antimicrobial peptides
NMR structural biology
Peptide structures
Membrane disruption
Helical peptides
Serum stability

ABSTRACT

The rapid emergence of resistant bacterial strains has made the search for new antibacterial agents an endeavor of paramount importance. Cationic antimicrobial peptides (AMPs) have the ability to kill resistant pathogens while diminishing the development of resistance. Citropin 1.1 (**Cit 1.1**) is an AMP effective against a broad range of pathogens. 20 analogues of **Cit 1.1** were prepared to understand how sequence variations lead to changes in structure and biological activity. Various analogues exhibited an increased antimicrobial activity relative to **Cit 1.1**. The two most promising, **AMP-016** (W3F) and **AMP-017** (W3F, D4R, K7R) presented a 2- to 8-fold increase in activity against MRSA (both = 4 μg/mL). **AMP-017** was active against *E. coli* (4 μg/mL), *K. pneumoniae* (8 μg/mL), and *A. baumannii* (2 μg/mL). NMR studies indicated that **Cit 1.1** and its analogues form a head-to-tail helical dimer in a membrane environment, which differs from a prior study by Sikorska et al. Active peptides displayed a greater tendency to form α-helices and to dimerize when in contact with a negatively-charged membrane. Antimicrobial activity was observed to correlate to the overall stability of the α-helix and to a positively charged *N*-terminus. Biologically active AMPs were shown by SEM and flow cytometry to disrupt membranes in both Gram-positive and Gram-negative bacteria through a proposed carpet mechanism. Notably, active peptides exhibited typical serum stabilities and a good selectivity for bacterial cells over mammalian cells, which supports the potential use of **Cit 1.1** analogues as a novel broad-spectrum antibiotic for drug-resistant bacterial infections.

1. Introduction

The emergence of drug resistant bacteria has made the development of novel antibacterial agents a pressing issue [1]. In fact, most experts consider bacterial infections one of the greatest threats to human health, which may result in more than 10 million deaths worldwide by 2050 [2]. Bacterial resistance to common antibiotics occurs through a variety of mechanisms [3]. For example, the Gram-positive pathogen methicillin resistant *Staphylococcus aureus* (MRSA) copes with antibiotic agents by increasing its membrane thickness or altering penicillin binding proteins (PBP) [4]. Gram-negative bacteria such as E*nterobacter* spp., *Escherichia coli*, *Klebsiella pneumoniae*, and *Pseudomonas aeruginosa* present resistance by virtue of a double membrane, by the development of efflux pumps, by the production of degrading enzymes, by gene transfer or by altering drug binding targets [5,6]. Antimicrobial peptides (AMPs) are an interesting option for combating resistant bacteria

Abbreviations: ALLOC, allyloxycarbonyl; AMP(s), antimicrobial peptide(s); CFU, colony forming unit; Cit 1.1, Citropin 1.1; CLint, *in vitro* intrinsic clearance; Dab, 2,4-diaminobutyric acid; DFQ-COSY, double quantum filtered COSY; Dpr, 2,3-diaminopropionic acid; Fmoc, fluorenylmethyloxycarbonyl; Gd-DTPA, gadolinium-diethylenetriamine pentaacetic acid; HMDS, hexamethyldisilazane; IC_{50}, half maximal inhibitory concentration; MIC, minimum inhibitory concentration; Orn, ornithine; PMDS, polydimethylsiloxane; PSVS, protein structure validation software; Sar, sarcosine; SEM, scanning electron microscopy; TMSP, trimethylsilylpropanoic acid; TOCSY, TOtal Correlated Spectroscopy

* Corresponding author at: Department of Chemistry, University of Nebraska – Lincoln, NE, 68588-0304, USA.
** Corresponding author. Department of Pharmaceutical Sciences, University of Nebraska Medical Center – Omaha, NE, 68198-6125, USA.
E-mail addresses: rpowers3@unl.edu (R. Powers), martin.condasheridan@unmc.edu (M. Conda-Sheridan).
[1] Equal contribution.

https://doi.org/10.1016/j.peptides.2019.170119
Received 15 May 2019; Received in revised form 9 July 2019; Accepted 13 July 2019
Available online 20 July 2019

to conventional small molecule antibiotics [7]. AMPs are capable of killing a wide range of microorganisms by membrane pore formation, or membrane disruption. In addition, AMPs can present antibacterial activity by inhibiting protein synthesis, enzymatic activity, or cell wall synthesis [8–10]. The most attractive feature of AMPs is the observation that bacteria are less likely to develop resistance to AMPs when compared to non-peptide antibiotics [11]. This stems from the fact that the fundamental structure of the membrane is not easily altered by mutations. In order to develop AMPs as antimicrobial agents it is essential to determine its mechanism of action and the structural features that give rise to their activities. This understanding is key to improving and evolving their efficacy.

Citropin 1.1 (**Cit 1.1/AMP-001**) is an AMP derived from the skin of an Australian tree frog of the *Litora* genus. **Cit 1.1** has shown intriguing activity against Gram-positive and Gram-negative species including: *Staphylococcus aureus*, *Staphylococcus epidermis, Enterococcus faecalis, Escherichia coli,* and *Klebsiella pneumonia* [12]. Conversely, studies evaluated the antifungical activity of **Cit 1.1** against *Candida* species using direct bioautography [13] and against *Candida albicans*, *Candida tropicalis* and *Candida krusei* isolated from patients with oral cavity and respiratory tract infections [14]. They found that the peptide was weekly active and less potent than amphotericin B and nystatin against clinical strains [13,14]. To our acknowledge, **Cit 1.1** has not been further tested against any other fungal strains besides *Candida* ssp., suggesting the antifungal potential of this peptide and its analogues can be further explored.

Previous structure-activity relationship (SAR) reports indicated that truncation of **Cit 1.1** sequence, such as deletion of Gly1, Leu2, or Phe3, completely ablated the peptide's activity. On the other hand, deletion of Gly14, Gly15, or Leu16 had no impact on **Cit 1.1** activity [15]. Tyler and co-workers suggested that the α-helical conformation of **Cit 1.1** was critical to antimicrobial activity [16]. In fact, replacement of the L-amino acids with their D-isomers yielded an AMP with similar biological activity [16]. Later studies showed that if an isoAsp bond is formed between Leu5 and the carboxylic acid side chain of Asp4 biological activity is abolished while the serum stability is greatly enhanced [17]. This conformational change does not affect the total charge of **Cit 1.1** and only marginally changes the isoelectric point and hydrophobicity; however, an isoAsp bond significantly alters its secondary structure hinting to the importance of the peptide's conformation [17]. It has been additionally proposed that two α-helices are formed upon contact of **Cit 1.1** with bacterial membranes [15]. Accordingly, an α-helical structure for **Cit 1.1** appears to play an important role in the peptide's antimicrobial activity. It is important to note that these prior studies relied on the introduction of relatively large structural changes to investigate a relationship between amino acid composition and peptide conformation on biological activity.

In this report, we sought to develop new **Cit 1.1** analogues enhanced antimicrobial action against various pathogens. Further, we expanded upon the previous structural investigations by further characterizing the conformation and interactions of **Cit 1.1** and its analogues in a membrane mimetic environment. The membrane-bound solution structures of the **Cit 1.1** peptides were determined using nuclear magnetic resonance (NMR) spectroscopy. The mode of membrane disruption was visualized using transmission and scanning electron microscopy techniques (TEM and SEM), flow cytometry and confocal microscopy. The toxicity of the most potent AMP was studied *in vitro* against mammalian and human red blood cells. Poor serum stability of peptide-based antimicrobials is another factor limiting the use of AMPs and, therefore, we have also studied the serum stability of **Cit 1.1** and its analogs. The experimental data has enabled us to define a mechanism of action for **Cit 1.1**, to describe the structural arrangement of the peptide when in contact with membranes, and to understand the impact of subtle molecular and conformational changes on peptide activity.

Table 1
Antimicrobial activities of **Cit 1.1 (AMP-001)** and AMP analogs.

Minimal inhibitory concentration (MIC) μg/mL				
Peptide sequence	Peptide code	Sa[a]	Ec[b]	LogP[c]
GLFDVIKKVASVIGGL	AMP-001/ Cit 1.1	32	32	−3.60
SarLFDVIKKVASVIGGL	AMP-002	32	64	−3.17
AcGLFDVIKKVASVIGGL	AMP-003	≥256	≥256	−3.78
$(CH_3)_3$GLFDVIKKVASVIGGL	AMP-004	≥256	≥256	−6.14
Hydrazine-LFDVIKKVASVIGGL	AMP-005	≥256	≥256	−2.50
GLFDVI(Orn)(Orn)VASVIGGL	AMP-006	> 32[d]	32	−4.49
GLFDVI(Dab)(Dab)VASVIGGL	AMP-007	> 32	32	−5.52
GLFDVI(Dpr)(Dpr)VASVIGGL	AMP-008	> 32	64	−5.64
GLFDVI(Cit)KVASVIGGL	AMP-009	128	256	−4.56
$(CH_3)_3$GLFDVIK$(CH_3)_3$K $(CH_3)_3$VASVIGGL	AMP-010	≥256	≥256	−13.64
GLFDVIK$(CH_3)_3$K$(CH_3)_3$VASVIGGL	AMP-011	≥256	≥256	−10.29
GLFDVIRRVASVIGGL	AMP-012	16	32	−5.16
GLFDVIRKVASVIGGL	AMP-013	16	> 32	−4.38
GLFDVIKKGVASVIGGL	AMP-014	≥256	64	−4.71
GLFEVIKKVASVIGGL	AMP-015	> 32[d]	> 32	−3.31
GLWDVIKKVASVIGGL	AMP-016	8	16	−3.50
GLWRVIRKVASVIGGL	AMP-017	16	32	−4.55
PhenylGlyLWDVIRKVASVIGGL	AMP-018	16	> 32	−2.34
GL(Biphenylalanine)DVIKKVASVIGGL	AMP-019	8	32	−1.85
GL(1-Nap)DVIKKVASVIGGL	AMP-020	8	64	−2.61
SarLWDVIRKVASVIGGL	AMP-021	Ne	Ne	−3.85

[a] *Staphylococcus aureus* JE2 MRSA.
[b] *Escherichia coli* K12.
[c] Calculated from MarvinSketch Version 14.9.
[d] 64.

2. Results

2.1. Minimum inhibitory concentration (MIC assay)

Cit 1.1 analogues were prepared using solid phase peptide synthesis (SPPS). Table 1 shows the amino acid sequence of the synthesized peptides and the observed MIC values against *S. aureus* JE2 (MRSA) and *E. coli* K12 (see **Experimental S5** for detailed procedures). **Cit 1.1** (**AMP-001**) displayed activity against MRSA (32 μg/mL) and *E. coli* (32 μg/mL) corroborating findings from previous studies (Table 1) [16,18,19]. **Cit 1.1**, however, did not demonstrate any activity against *Acinetobacter baumannii*, *Candida albicans* or *Cryptococcus neoformans* (Table 2). **AMP-002** with a methyl glycine (sarcosine, Sar1) substituent retained activity against *S. aureus* (32 μg/mL) but exhibited diminished activity against *E. coli* (64 μg/mL). The acetylation (**AMP-003**), the methylation to yield the quaternary ammonium analogue (**AMP-004**), or substitution by a hydrazine group (**AMP-005**) at the *N*-termini of **Cit 1.1** eliminated antibacterial activity (MIC ≥ 256 μg/mL).

Replacing the Lys residues (Lys7, Lys8) with ornithine (Orn), 2,4-diaminobutyric acid (Dab), or 2,3-diaminopropionic acid (Dpr) yielded analogues **AMP-006**, **AMP-007** and **AMP-008**, respectively. These changes diminished the potency against Gram-positive pathogen when compared to **Cit 1.1** (Table 1). The peptides displayed equal (**AMP-006** and **AMP-007**, 32 μg/mL) or reduced antibacterial action (**AMP-008**, > 32 μg/mL) against Gram-negative bacteria. On the **AMP-009** analogue Lys7 was replaced with citrulline, which substitution resulted in a lack of antibacterial activity. **AMP-010** was synthesized by methylating all of the available **Cit 1.1** amine groups, whereas **AMP-011** was generated by methylating the Lys amine moieties to produce analogues with a resident positive charge. Both **AMP-010** and **AMP-011** exhibited a complete lack of antibacterial activity. **AMP-012** was constructed by replacing Lys7 and Lys8 with arginine residues, while the **AMP-013** analogue was prepared by only substituting Lys7 for an arginine. The MICs for both **AMP-012** and **AMP-013** decreased 2-fold against the MRSA strains (16 μg/mL) while the activity against Gram-

Table 2
Additional antimicrobial activities of **Cit 1.1 (AMP-001)** and selected AMP analogs.

Minimal inhibitory concentration (MIC) μg/mL								
Peptide sequence	Peptide code	Sa[a]	Ec[b]	Pa[c]	Kp[d]	Ab[e]	Ca[f]	Cn[g]
GLFDVIKKVASVIGGL	AMP-001/Cit 1.1	32	> 32	> 32	> 32	32	> 32	16
GLFDVI(Orn)(Orn)VASVIGGL	AMP-006	32	> 32	> 32	> 32	> 32	> 32	32
GLFDVIRRVASVIGGL	AMP-012	16	32	> 32	> 32	32	16	16
GLFDVIRKVASVIGGL	AMP-013	16	> 32	> 32	> 32	32	> 32	16
GLFEVIKKVASVIGGL	AMP-015	32	> 32	> 32	> 32	> 32	> 32	16
GLWDVIKKVASVIGGL	AMP-016	4	> 32	> 32	> 32	16	32	8
GLWRVIRKVASVIGGL	AMP-017	4	4	> 32	8	2	32	2
PhenylGlyLWDVIRKVASVIGGL	AMP-018	8	> 32	> 32	> 32	32	32	8
GL(Biphenylalanine)DVIKKVASVIGGL	AMP-019	4	32	> 32	> 32	16	32	> 32
GL(1-Nap)DVIKKVASVIGGL	AMP-020	4	32	> 32	> 32	16	32	> 32
SarLWDVIRKVASVIGGL	AMP-021	8	16	> 32	32	4	32	16

[a] *Staphylococcus aureus* ATCC 43300 MRSA.
[b] *Escherichia coli* ATCC 25922.
[c] *Psedomonas aeruginosa* ATCC 27853.
[d] *Klebsiella pneumoniae* ATCC 700603.
[e] *Acinetobacter baumannii* ATCC 19606.
[f] Candida albicans ATCC 90028.
[g] Cryptococcus neoformans var. grubii H99 ATCC 20882.

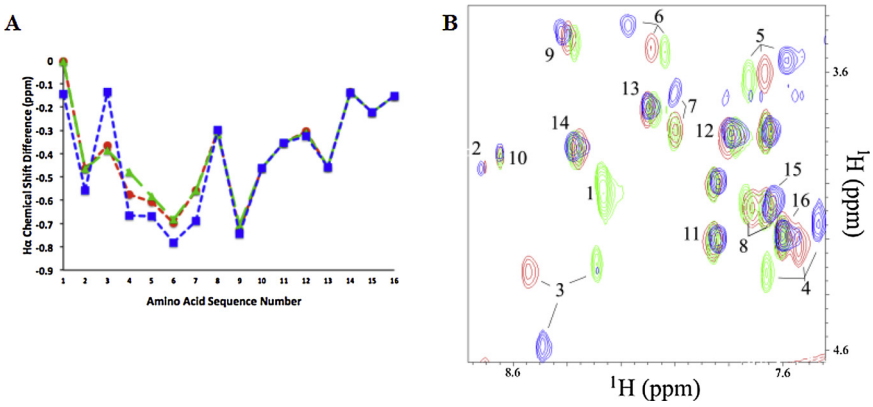

Fig. 1. (A) Plot showing the Hα deviations (ppm) from statistical-coil chemical shifts. Amino acids are numbered according to their sequence in **Cit 1.1** (red), **AMP-003** (green), and **AMP-016** (blue). (B) TOCSY Hα region for **Cit 1.1** (red), **AMP-003** (green), and **AMP-016** (blue). Peaks are labeled according to their respective amino acid position.

negative organisms was retained or diminished (MIC > 32 μg/mL) when compared to **Cit 1.1** (Table 1 and **2**). Interestingly, **AMP-012** and **AMP-013** exhibited antifungal activity with a MIC of 16 μg/mL against *C. neoformans* while **AMP-012** displayed MIC of 16 μg/mL against *Candida albicans* (Table 2). A glycine residue was then inserted following Lys 8, in order to alter the relative position of potentially key α-helical residues. **AMP-014** was observed to be inactive against the tested bacterial strains. The **AMP-015** analogue was designed with a modest substitution of Asp4 for Glu. Surprisingly, **AMP-015** was inactive against all bacterial strains tested (MIC > 32 μg/mL) but inhibited the growth of *C. neoformans* with a MIC of 16 μg/mL.

The **AMP-016** analogue was constructed by replacing Phe3 with Trp, which yielded an AMP with improved antibacterial activity against MRSA with MIC values of 8 μg/mL and 4 μg/mL for *S aureus* JE2 and *S aureus* ATCC 43300, respectively. **AMP-016** also exhibited a better antibacterial activity against *E. coli* K12 with an MIC value of 16 μg/mL. **AMP-016** did not demonstrate antibacterial activity against *K. pneumoniae* or *P. aeruginosa*, but it was active against *A. baumannii* (16 μg/mL), *C. albicans* (32 μg/mL) and *C. neoformans* (8 μg/mL). The Asp4 and Lys7 residues where changed to Arg in the **AMP-017** analogue, producing the most potent analogue of the series which was effective against MRSA and *E. coli* (MIC 4 μg/mL), *K. pneumoniae* (MIC 8 μg/mL) *A. baumannii* (MIC 2 μg/mL). **AMP-017** was also active against fungi with a MIC of 2 μg/mL against *C. neoformans*. Replacement of Gly1 with PhenylGly (**AMP-018**), Phe3 with a biphenylalanine residue (**AMP-019**), or 1-Naphyl (**AMP-020**) resulted in AMPs with improved antimicrobial activity against bacteria and fungi, when compared with the lead compound. For example, the MIC against MRSA was between 4–8 μg/mL. **AMP-019** and **AMP-020** were also active against the dangerous *A. baumannii* with MIC = 16 μg/mL. Gly1 was replaced with Sar to yield the **AMP-021** analog, which presented promising MIC values against MRSA (8 μg/mL), *E. coli* (16 μg/mL), *A. baumannii* (4 μg/mL) and *C. neoformans* (16 μg/mL).

2.2. NMR spectroscopy

Negatively charged sodium dodecyl sulfate (SDS) micelles, which mimics the charge of Gram-positive bacterial membranes, were therefore chosen as a model for the structural elucidation of **Cit 1.1**, **AMP-003**, and **AMP-016** peptides by NMR [20]. Standard two-dimensional (2D) TOCSY and NOESY datasets were collected for backbone and side-chain resonance assignments [21]. NMR assignments for **Cit 1.1**, **AMP-003**, and **AMP-016** were nearly complete with 94% HN, 100% Hα, 100% Hβ, 88% Hγ, 90–100% Hδ, 60–100% Hε, 0–33% Hζ, and 100% Hη of the assignments made (**Table S7**). Fig. 1A shows the Hα chemical shift deviations from statistical-coil values for the three peptides bound to SDS micelles [22,23]. The three peptides showed negative chemical shift differences across the entirety of the sequence, which is strongly suggestive of an α-helical conformation along the SDS micelle. Chemical shift differences between the **Cit 1.1**, **AMP-003**, and **AMP-016** peptides were more apparent when HN chemical shifts were included. This is illustrated by an overlay of the Hα region of the 2D TOCSY

spectra for the three peptides as shown in (Fig. 1B). Major chemical shifts changes were observed for residues 3 to 7, which are consistent with the Hα chemical shift changes plotted in Fig. 1A. In order to reinforce this observation, we performed circular dichroism (CD) studies. It was found the AMPs, presented α-helical character (with some random coils) in aqueous media (Fig. S6). The secondary structure of **AMP-016** was also studied after 1 h incubation with *E. coli* and the data showed the conformation was retained upon interaction with the bacteria membrane (Fig. S7).

The NMR structures for the **Cit 1.1**, **AMP-003**, and **AMP-016** peptides in SDS micelles were determined to further elucidate the role that structure plays in antimicrobial activity. The structural statistics for the three peptides (**Table S8**) indicates that the experimental data agrees well with the calculated structures. Backbone RMSDs for each of the peptides was 0.3 Å, 0.7 Å, and 0.4 Å for **Cit 1.1**, **AMP-003**, and **AMP-016**, respectively. The structures did not contain any NOE violations > 0.5 Å or dihedral angle violations > 5°. The high quality of the NMR structures is also evident by the PROCHECK z-scores of -0.3, -0.95, and -0.47 for **Cit 1.1**, **AMP-003**, and **AMP-016**, respectively [24]. Further, 92–94% of all residues are located in the most favored region of the Ramachandran plot. An overlay of the water refined 20 lowest energy NMR structures for the **Cit 1.1**, **AMP-003**, and **AMP-016** peptides are shown in Fig. 2A–C.

The resulting NMR structures indicate that the **Cit 1.1**, **AMP-003**, and **AMP-016** peptides adopt a head to tail helical dimer (Fig. 2D–F). The head to tail orientation of the peptides was confirmed by the presence of NOEs from Leu2 of strand **A** to Ile13/Leu16 of strand **B**. These long-range structural restraints are only possible for a head to tail dimer. Of particular note, a significant number of NOEs exist at the *N*-terminus (Fig. 2G, H), which is consistent with the presence of both an α- and 3_{10}-helix for the biologically active peptides (**Cit 1.1** and **AMP-016)**. It is possible that the peptides adopt both conformations (or are in equilibrium) when bound to a SDS micelle. In this case, the NMR structure would simply represent an overall average of the conformational exchange. Importantly, the inactive **AMP-003** lacks a similar NOE pattern (and number of NOEs) at the *N*-terminus and, thus, it exclusively adopts an α-helical structure (Fig. 2I). Since the only difference between **Cit 1.1** and **AMP-003** is the *N*-terminal acetylation, this clear difference in helix composition between the peptides is due to the acetylation.

Amide proton temperature titrations up to 70 °C were performed on the three peptides to characterize helical stability (Figs. S9–11). The titration data was binned according to the relative magnitude of the HN chemical shift changes ($\Delta^{H}N$): minor (0 to −0.05, yellow), intermediate (−0.05 to −0.25, orange), and major (−0.25 to −0.45, red). The peptide ribbon diagrams in Fig. 2D–F are colored based on these HN chemical shift changes in order to qualitatively assess the thermal stability of the helices. Amino acid residues exhibiting major chemical shift changes upon heating are transitioning from a stable and structurally-ordered state to a disordered and unstructured state. Conversely, residues with relatively unchanged chemical shifts are likely already in a transiently disordered state at room temperature.

Next the peptides were titrated with gadolinium-diethylenetriamine pentaacetic acid (Gd-DTPA) and monitored by NMR to identify the solvent exposed residues while the peptide was bound to SDS micelles (Figs. S12–14). The addition of a paramagnetic species will reduce the NMR signal intensity for residues in contact with the solvent proportionally to the amount of the added paramagnetic species. Upon the addition of Gd-DTPA, the majority of the amino acids exhibited an approximate linear decrease in peak intensity regardless of location in

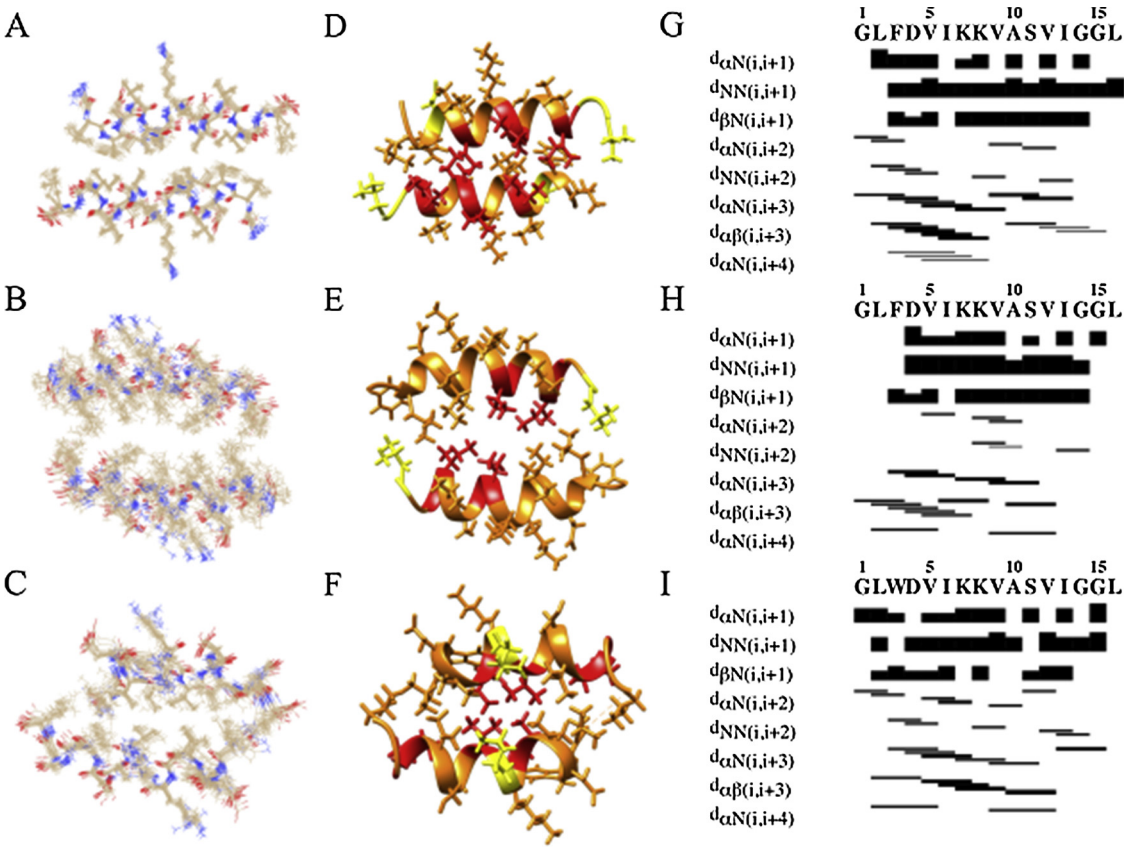

Fig. 2. The ensemble of the lowest energy, water refined structures of (A) **Cit 1.1**, (B) **AMP-003**, and (C) **AMP-016**. Peptide ribbon structures for (D) **Cit 1.1**, (E) **AMP-003**, and (F) **AMP-016** are colored by the binned amide proton temperature titration data according to the ΔH ranges 0 to −0.05 (minor chemical shift, yellow), −0.05 to −0.25 (intermediate chemical shift, orange), and −0.25 to −0.45 (major chemical shift, red). NOE connectivity plots for (G) **Cit 1.1**, (H) **AMP-003**, and (I) **AMP-016**. Weights of the connectivities are normalized to the NOE intensities.

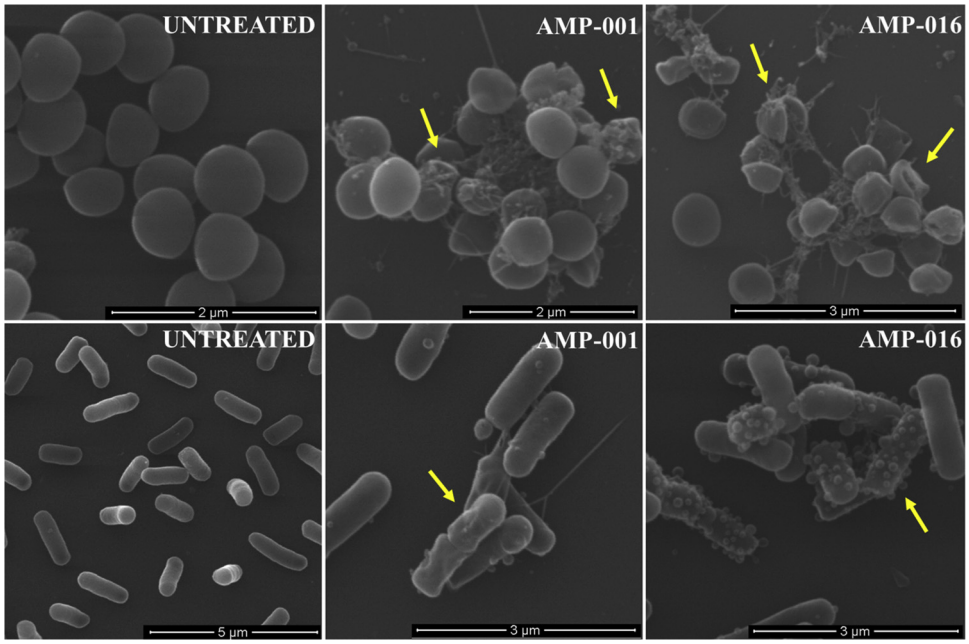

Fig. 3. SEM micrographs of *S. aureus* JE2 MRSA (*top row*) and *E. coli* K12 (*bottom row*) cells treated with either **Cit 1.1** or **AMP-016** at twice the MIC reported in Table 2.

the dimer structure. This is most likely due to multiple binding sites for Gd-DTPA on each peptide, an aggregation of the peptides along the surfaces of the micelles, and a dynamic association/dissociation of the dimer [25]. Leu2 in **Cit 1.1** and **AMP-016** was an exception to this general observation. The NMR peak intensity for Leu2 increased, at first, with the addition of Gd-DTPA. Of note, the peak intensity for Leu2 was relatively weak compared to the other residues (Fig. 1B), which is suggestive of a high exchange rate and/or a transiently disordered structure.

2.3. Scanning electron microscopy (SEM)

S. aureus JE2 and *E. coli* K12 cells were treated for 1 h with **Cit 1.1** or **AMP-016** at 2X MIC values. As clearly evident from the SEM images, AMP treatment led to membrane disruption accompanied by cytoplasmic leakage, deep holes and severe membrane deformations (Fig. 3). These morphological changes indicate that the AMPs kill bacteria by disrupting cell membranes, although the results do not exclude additional mechanisms of action. Please note the SEM micrographs present some differences between *S. aureus* and *E. coli*, which may suggest a different mechanism of action for AMP antimicrobial activity between Gram-positive and Gram-negative organisms. In the case of *S. aureus,* holes and cytoplasm release were observed. Conversely, membrane solubilization due to a mixed peptide/phospholipid vesicle formation (budding) with subsequent membrane thinning leading to only a small amount of cytoplasm release was observed for *E. coli.*

2.4. Propidium iodide (PI) uptake and flow cytometry

A PI uptake assay was performed to confirm the ability of AMPs to disrupt bacterial cell membranes. *S. aureus* JE2 and *E. coli* K12 cells were treated with **Cit 1.1** or **AMP-016** at 2X MIC values. The PI fluorescence intensity was measured relative to Polymyxin B (PMB) as a reference. **Cit 1.1** and **AMP-016** showed high PI uptake relative to controls (Fig. 4), further suggesting that bacterial cell death is associated with membrane damage, since PI can only cross damaged cell membranes. The cell membrane disruption of *S. aureus* JE2 and *E. coli* K12 was further evaluated with flow cytometry. Untreated (no AMPs)

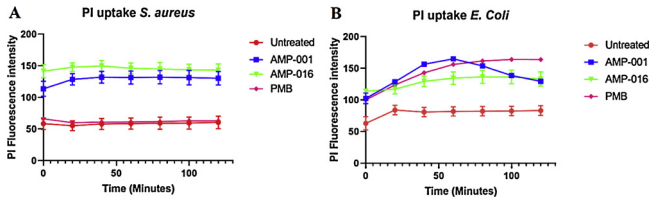

Fig. 4. PI uptake of AMPs. *S aureus* JE 2 (A) and *E. coli* K12 (B) cells (1×10^7 CFU) were untreated, treated with AMPs (2xMIC) or treated with Polymixyn B (PMB, 16 µg/mL) for 120 min. The PI fluorescence intensity was then measured at 20 min intervals for a total of 120 min. PMB is known to kill Gram-negative bacteria by disrupting cell membrane and was used as a positive control.

and treatment with 70% EtOH were used as negative and positive controls, respectively (Experimental S15 and Fig. S16). After 1 h treatment with either **Cit 1.1** or **AMP-016** at 2X MIC values, *S. aureus* cells showed an increased uptake, when compared to control, of 9.4% or 12.5%, respectively (Fig. S16). Similarly, *E. coli* cells treated with either **Cit 1.1** or **AMP-016** exhibited cell viability of 13.9% or 27.5%, respectively.

2.5. In vitro serum stability

Serum stability was assessed by incubating the peptides in human serum for over two hours followed by quantitation using LC–MS/MS. **AMP-002** and **-006** displayed the highest serum stability. Approximately 60%–80% of the peptides remained in the serum after 2 h. **Cit 1.1, -012, -013,** and **-016** displayed similar stabilities with only 40–50% of the peptide remaining in the serum after 2 h (Fig. 5).

2.6. Cytotoxicity

The cytotoxicity of the active AMPs against human embryonic kidney cells (ATCC CRL-1573) was performed using a resazurin test and the IC_{50} values were determined from dose response curves. The hemolytic activity was determined against human red blood cells and the HC_{50} values (concentration at 50% hemolysis) were calculated by curve fitting of the inhibition values *versus* log(concentration). The IC_{50} and HC_{50} values are summarized in Table 3. In general, the AMPs showed

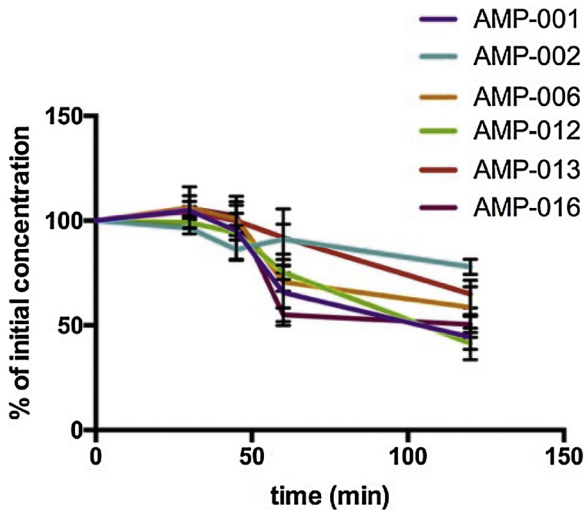

Fig. 5. Stability of **Cit 1.1** and the AMP Analogues in Human Serum studied by LC–MS. AMP serum concentrations are normalized to initial concentrations (0 min, 100% AMP). The data is plotted as mean ± SD from triplicate measurements.

Table 3
AMP cytotoxicity and hemolytic activity.

Peptide sequence	Peptide code	IC_{50} (μg/mL) HEK-293[a]	HC_{50} (μg/mL) Human red blood cells
GLFDVIKKVASVIGGL	AMP-001/ Cit 1.1	20.98	> 32
GLFDVI(Orn)(Orn)VASVIGGL	AMP-006	> 32	> 32
GLFDVIRRVASVIGGL	AMP-012	17.64	18.2
GLFDVIRKVASVIGGL	AMP-013	21.26	> 32
GLFEVIKKVASVIGGL	AMP-015	> 32	> 32
GLWDVIKKVASVIGGL	AMP-016	> 32	16.85
GLWRVIRKVASVIGGL	AMP-017	18.10	26.7
PhenylGlyLWDVIRKVASVIGGL	AMP-018	19.44	> 32
GL(Biphenylalanine)DVIKKVASVIGGL	AMP-019	17.04	> 32
GL(1-Nap)DVIKKVASVIGGL	AMP-020	16.85	> 32
SarLWDVIRKVASVIGGL	AMP-021	30.90	> 32

[a] Human embryonic kidney cells (ATCC CRL-1573). Assays were performed by The Community for Antimicrobial Drug Discovery (CO-ADD), Australia.

IC_{50} values between 6.8 and 30.9 μg/mL. **AMP-012**, **AMP-016** and **AMP-017** were exceptions and displayed IC_{50} values higher than 32 μg/mL. In addition, most of the AMPs exhibited low hemolytic activity with HC_{50} values greater than 32 μg/mL. **AMP-006**, **AMP-015** and **AMP-016** were exceptions and displayed lower HC_{50} values corresponding to 18.2 μg/mL, 16.8 μg/mL and 26.7 μg/mL, respectively.

3. Discussion

3.1. Antimicrobial activity

We have rationally designed analogues of the AMP **Cit 1.1** to understand the contribution of sequence and structure to its antibacterial activity. The *N*-terminus of AMPs tend to be polar or ionic, which is likely to play a key role in membrane interactions [11]. In the **AMP-002** analogue Gly1 was replaced with a methyl glycine. This change should increase serum stability [26] and the lipophilicty at the *N*-terminus. The compound exhibited comparable activity to **Cit 1.1** against *S. aureus* JE2, but was half as potent against *E. coli* K12, which suggests multiple H-bond donors may be needed at the *N*-terminus of AMPs for full activity. This is consistent with the results obtained with the **AMP-003** analog, which is acetylated at the *N*-terminus. Acetylation of amines alters the pK_a (preventing protonation) and the isoelectric point while also reducing the net charge of the peptide [27].

To further investigate the importance of the primary amine on **Cit 1.1** activity, the *N*-terminus was converted into a quaternary amine (**AMP-004**). This was based on the notion that resident positive charges aid antibacterial activity [28,29]. This modification was expected to have two distinct impacts on **Cit 1.1** because: (1) a permanent positive charge is pH-independent, but cannot form a hydrogen bond; (2) the quaternary amine makes the AMP more resistant to proteolysis, which increases its bioavailability [30]. Unexpectedly, **AMP-004** was observed to be inactive against *S. aureus* and *E. coli*, indicating that a positive charge on the *N*-terminal amine is not enough to interact with bacterial membrane. This suggests a role of H-bonding; either an interaction within the peptide (as suggested by others) or an association with the bacteria that is important for activity. Similarly, replacing Gly1 with a hydrazine group resulted in the loss of antibacterial activity for **AMP-005**. Hydrazines have a lower pKa (˜8.3) than amines (˜9.6), a value that should be further lowered by the neighboring electron-withdrawing group [31,32]. As a result, the hydrazine nitrogen may not protonated (note that the alkylated nitrogen is the most likely site of protonation [33]) under the conditions of the MIC assay. Furthermore, it is possible that an internal hydrogen bond may form between the hydrogen on the hydrazine and the amide carbonyl. In addition to preventing a hydrogen bond with the bacterial membrane, this internal hydrogen bond may also affect the overall peptide structure and alter its biological activity. The inactive **AMP-003**, **AMP-004** and **AMP-005** analogues clearly emphasize the importance of the *N*-terminus in AMP activity and the potential critical role that hydrogen bond donors and acceptors play in the interaction with the bacterial membrane. It is important to note that although our NMR data clearly established different NOE patterns at the *N*-terminus between the active and inactive peptides, the presence of NOEs do not necessarily confirm the presence or absence of a hydrogen bond. Therefore, the speculation on intramolecular hydrogen bond formation in the AMPs and at the membrane interface is primarily based upon the chemical structures of the *N*-terminal modifications.

AMPs usually contain two or more cationic side chains such as Lys and Arg, allowing for a potential electrostatic interaction with the bacterial membrane. Accordingly, several modifications to **Cit 1.1** were made to evaluate the role of these charged residues to antibacterial activity. Lys7 and Lys8 were replaced with progressively shorter amine bearing sidechains: Orn, Dab, and Dpr. This change was intended to diminish lipophilicty while instructing us of the role of charge projection within the α-helix. Replacing with Orn (**AMP-006)** resulted in diminished activity against MRSA JE2 while the inclusion of Dab (**AMP-007**) and Dpr (**AMP-008)** abolished the antibacterial against most of the tested pathogens. These findings suggest the longer side chain of Lys is necessary for membrane interaction and the antibacterial activity of **Cit 1.1**. Another possibility is that there is an optimal hydrophobic index as a decrease in $-CH_2$ units, results in lower hydrophobicity as seen by the LogP values (Table 1) of -4.49, -5.52, -5.64, and -3.60 for Orn, Dap, Dpr and **Cit 1.1**. Nevertheless, a direct correlation between LogP values and antibacterial activities was not observed across the series. Indicating antibacterial activities is dependent on a combination of multiple factors.

The Lys residues were methylated to explore the relative contribution of electrostatic interactions and hydrogen bonds to biological activity. Unexpectedly, and despite having a permanent +3 charge, both **AMP-010** and **AMP-011** were found to be inactive. This result implies a H-bond donor is key to the biological activity of **Cit 1.1** and its analogs.

Arginine-rich peptides have also been shown to exhibit potent antibacterial activity [34,35]. In fact, a number of studies have indicated that an increase in arginine *versus* lysine content results in higher antimicrobial action [36,37]. To investigate this, a **Cit 1.1** analogue (**AMP-012)** was constructed where Lys7 and Lys8 were replaced with an arginine. An **AMP-013** analogue was also prepared that only

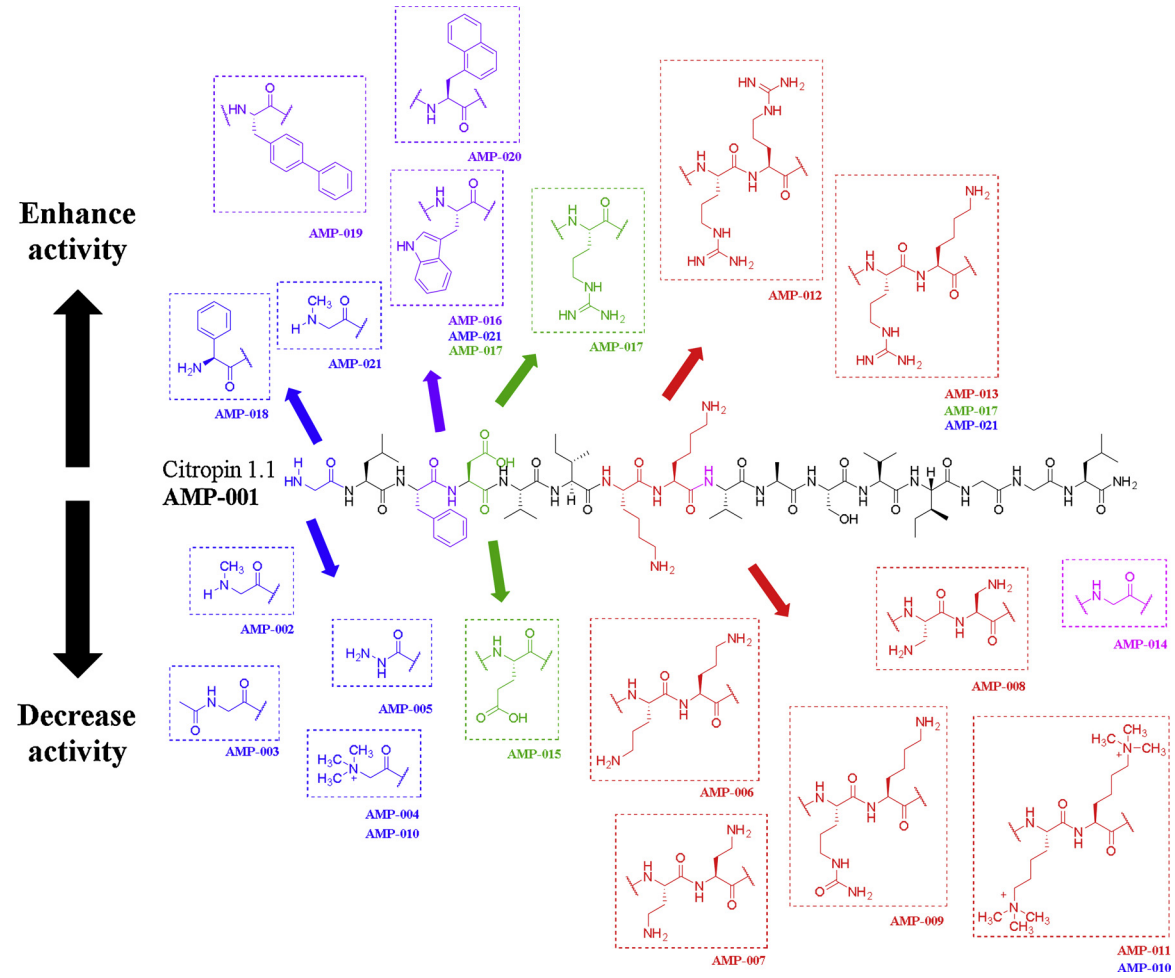

Fig. 6. Summary of the **Cit 1.1** SAR.

replaced Lys7 with an arginine. The MICs for both **AMP-012** and **AMP-013** decreased 2-fold against *S. aureus* to 16 μg/mL. The increase in antimicrobial activity may be explained by an enhanced translocation of peptides within the *S. aureus* cells [38,39]. However, the **AMP-012** and **AMP-013** displayed diminished activity against most of the Gram-negative organisms tested. Interestingly, **AMP-012** exhibited antifungal activity against both *C. albicans* and *C. neoformans* (16 μg/mL). To further explore the importance of cationic residues on activity, citrulline a structural mimic of arginine containing a urea functional group instead of the charged guanidium group was constructed (**AMP-009**). This substitution resulted in a complete lack of antibacterial activity, further establishing the importance of a charged H-bonding donor at position 7 (the citrulline urea group is capable of forming a hydrogen bond but its side chain is uncharged). The citrulline substitution reduces the net charge of **AMP-009**, which suggests the net charge of the peptide also contributes to the antimicrobial activity of AMPs.

Previous studies have shown that **Cit 1.1** adopts an α-helical conformation, but there has also been some conflicting evidence about the exact details of the **Cit 1.1** structure [15]. Instead of a single α-helical chain, two helices have been suggested for the **Cit 1.1** structure [15]. To address this possibility, a glycine residue was inserted into the **Cit 1.1** sequence following Lys8 to create the **AMP-014** analog. The insertion of Gly9 was expected to provide added flexibility to the peptide [40,41] and potentially enhance its activity if the two-helix model was correct. **AMP-014** was observed to be inactive against all the bacterial strains tested and suggests the two-helix model for **Cit 1.1** may be incorrect. If the **Cit 1.1** structure is comprised of two α-helices separated by a flexible link, then the inserted Gly may allow enough mobility for the correct surface of the α-helices to interact with the membrane. Nevertheless, it is important to note the Gly insertion lengthens the peptide and shifts the sequence beyond Lys8 affecting the charge distribution at the **Cit 1.1** surface. Thus, the loss in activity may also be explained by a change in the position of the hydrophobic and charged residues.

The **AMP-015** analog, which contains a Glu for Asp4 substitution, was also inactive. Others have suggested a potential H-bond between the *N*-terminus and residue 4 [16]. This change may affect such interaction but no change in activity was observed. **AMP-016** was constructed by replacing Phe3 with Trp. Tryptophan-rich peptides have been shown to enhance the activity of AMPs presumable due to a larger hydrophobic area [34,42] and the insertion of Trp residues at the membrane-water interface [41]. The **AMP-016** analogue exhibited a 4-fold and 2-fold increase in activity against *S. aureus* and *E. coli*, respectively. In addition, **AMP-016** was active against *C. neoformans* (8 μg/mL). Thus, we think the indole ring in tryptophan is likely acting as a better anchor to the bacterial membranes than the smaller phenyl ring [42].

AMP-017, **AMP-018** and **AMP-21** were designed to maintain the increased antimicrobial activity resulting from the inclusion of Trp at position 3, while investigating the impact of other amino acid substitutions at different positions. **AMP-017** (Asp4 and Lys7 were replaced by Arg) showed an increase in activity against *E. coli*, *K. pneumoniae*, *A. baumannii* and *C. neoformans* when compared with **Cit 1.1** or **AMP-016**. However, replacing Gly1 with PhenylGly and Lys7 with Arg (**AMP-018**) dramacticaly decreased the activity of AMP-017 against bacteria (still, this compound was better than **Cit 1.1**). **AMP-021**,

where Gly1 was replaced by Sar and Lys7 by Arg, showed a slight decrease in activity against Gram-negative strains that **AMP-017**. However, the molecule had better activity than **Cit 1.1** or **AMP-018**. This results indicate the key role of Trp3 or Arg4 on activity.

We also replaced Phe3 with other aromatic amino acids; biphenylalanine or naphthylalanine (**AMP-019 and AMP-020**). These replacements maintained the activity observed with **AMP-016** against *S. aureus,* while reducing activity against Gram-negative bacteria and fungi. The analogue was slighlty more potent than **Cit 1.1**. These finding may also be correlated to the increasing hydrophobicity (LogP -1.85, -2.61, and -3.60 for **AMP-019**, **AMP-020** and **Cit 1.1**, respctively) which may facilitate the peptide insertion into the bacteria membrane. Fig. 6 summarizes the structure-activity relationship for the series of AMP analogs.

3.2. NMR spectroscopy

Cit 1.1, **AMP-003**, and **-016** were analyzed by NMR to elucidate the relationship between structure and antimicrobial activity. Interestingly, Fig. 1A indicates that the largest H*a* chemical shift difference between the three peptides occurs at the *N*-terminus between residues Asp3 and Lys7. Although the dissimilarity between **AMP-016** and **Cit 1.1/AMP-003** can be attributed to the tryptophan substitution at position 3, the minor deviation of Asp4 is likely a result of the acetylation of the *N*-terminus. In the case of **AMP-016**, the steric and electronic effects from the indole side chain at position 3 may lead to a significant decrease in helicity. *N*-terminal acetylation does not induce any significant effect on the overall helicity of **AMP-003** except for a slight decrease at Asp4. The removal of the charged *N*-terminus changes the polarity or the hydrogen-bond network around Asp4, which contributes to a decrease in helicity. Fig. 1B shows the overlay of the Hα region of the 2D TOCSY for the three peptides. The significant chemical shift differences of the *N*-terminal residues highlight a changing local environment for residues 3 to 7 that is likely a result of minor alterations in the structure of the three peptides. Accordingly, these subtle changes in the peptide's structure may be directly related to differences in antimicrobial activity.

Our NMR derived structures for **Cit 1.1**, **AMP-003**, and **-016** differ from the previous results of Sikorska et al. that describe the presence of two helices within **Cit 1.1** structure [15]. Experimentally determined NOEs were found along the full length of each of the peptides **(**Fig. 2G–I**)** and between the helices in a dimer orientation. Although the **Cit 1.1**, **AMP-003**, and **AMP-016** dimers are not completely superimposable, there are no major structural differences between the three peptide structures that appear to explain the difference in activity. In all cases, the dimers pack together along a hydrophobic face, which then exposes charged residues to the solvent. Consequently, the peptides' NMR structures are consistent with the prior observation that the number and distribution of hydrophobic residues is crucial for antimicrobial activity [43]. Increasing peptide hydrophobicity increases antimicrobial activity, but only if the overall hydrophobicity remains below an optimal upper threshold. Peptide aggregation likely occurs if too many hydrophobic residues are inserted into the peptide sequence, which leads to a loss in activity. Therefore, the **Cit 1.1** peptide must maintain a hydrophobic surface to allow for a stable dimer in order to carpet a bacterial cell membrane, but must also avoid the formation of inactive aggregates. The tryptophan substitution in **AMP-016** and the corresponding increase in antimicrobial activity supports the above hypothesis. The hydrophobic and electrostatic properties of tryptophan [44] allows **AMP-016** to maintain a similar overall hydrophobicity to **Cit 1.1** while also promoting peptide aggregation at the membrane surface, and a positive electrostatic interaction with the negatively-charged membrane. This, however, does not explain the differences in activity between the active (**Cit 1.1/AMP-016**) and inactive (**AMP-003**) peptides since all of the peptides form a similar head-to-tail dimer. Instead, the primary difference between the active and inactive peptide dimers is the *N*-terminal acetylation.

It has been previously observed that *N*-terminal acetylation increases the propensity of α-helix formation in peptides regardless of the amino acid sequence [45]. *N*-terminal acetylation also increases the overall stability of an α-helix. In the case of **Cit 1.1**, the apparent increase in helical stability due to acetylation resulted in a loss of activity. Consequently, antimicrobial activity may be correlated with a certain amount of structural disorder or mobility within the peptide. Of course, this result can also be linked to the loss of basicity as explained earlier. The NMR also leads to the theory that antimicrobial activity may depend on an equilibrium between a disordered monomer in solution and helical dimers coating the membrane surface. In the presence of bacteria, the equilibrium shifts from disordered monomer to the helical dimer. The dimer is then able to associate with other dimers on the membrane surface and promote antimicrobial activity through a proposed carpet mechanism. However, if the peptide is stabilized in solution then the equilibrium is shifted away from interacting with the bacterial membrane and the antimicrobial activity is abolished. We hypothesize that **Cit 1.1** exists as a disordered monomer in solution and dimerizes and aggregates along the anionic surface of the bacterial membrane. In the inactive form, the *N*-terminal acetylation stabilizes the transiently formed α-helix in solution. Consequently, the aggregation on the membrane surface, which promotes antimicrobial activity, is greatly diminished. Again, the observation that the inactive **AMP-003** dimer is exclusively α-helical and the **Cit 1.1/AMP-016** dimers are a mixture of α- and 3_{10}-helix is supportive of the proposal that helix stability affects antimicrobial activity. To further investigate the role of α-helical stability in regard to antimicrobial activity, NMR was used to measure the thermal stability and solvent accessibility of the **Cit 1.1**, **AMP-003**, and **AMP-016** peptides.

The temperature-dependent chemical shift changes clearly define the dimer interface as the residues with the largest $\Delta^{H}N$ values (Figs. 2D–F, S1–3). The residues in the dimer interface correspond to: Ile6, Val9, Ala10, Ile13, and Gly14. Importantly, the inactive **AMP-003** peptide exhibited the smallest HN chemical shift changes for these residues. This suggests the inactive **AMP-003** is relatively less stable as a dimer in the SDS micelle compared to the active peptides. Interestingly, there are additional **AMP-003** residues outside of the dimer interface that also exhibit a temperature-dependent chemical shift change. This was not observed for the **Cit 1.1** or **AMP-016** peptides. One possible explanation for this difference is that the **AMP-003** peptide still maintains an α-helical structure as a monomer, which undergoes further temperature-dependent denaturation. This does not appear to occur for **Cit 1.1** or **AMP-016.** In fact, more residues in the **Cit 1.1** peptide compared to **AMP-003** are disordered based on the lack of a temperature-dependent chemical shift change. These results suggest that a certain amount of structural disorder or dynamics is necessary for antimicrobial activity.

The presence of a helical dimer is also suggested by the Gd-DTPA titration experiments. At low concentrations of Gd-DTPA, the amide peak intensity for Leu2 was found to increase, which indicates a reduction in the chemical exchange with the solvent. It is plausible that the coordination of Gd-DTPA by the active peptides stabilizes the dimer structure and reduces the amide chemical exchange of Leu2 causing an initial sharpening of the peak. Only at higher Gd-DTPA concentrations does the Leu2 NMR resonance broaden like the other amino acid residues. This effect is not seen in the inactive peptide (**AMP-003**), suggestive of a more stable α-helix along the entirety of the peptide monomer (Fig. S4–6).

3.3. Mechanism of action in bacteria membrane

Bacterial membrane disruption can be described by the worm-hole, the barrel-stave, or the carpet models [46,47]. Previously reported data on the **Cit 1.1** interaction with negatively charged lipid vesicles hinted towards involvement of the carpet mechanism [12]. In the carpet-

model of membrane disruption, the AMPs bind parallel to the bacterial membrane covering its entire surface. This causes cell membrane permeation and eventually release of small vesicles from the membrane [46,47]. A separate study involving giant unilamellar vesicles (GUVs) further supported the carpet mechanism proposed earlier [40]. Conversely, an atomic force microscopy study by Henderson and colleagues indicates that **Cit 1.1** can promote the formation of worm-like micelles, which could be an outcome of many toroidal pore formations [48]. However, those prior studies relied on negatively charged phospholipid model membranes, which are structurally simple compared to bacterial membranes. These model membranes do not accurately represent the complexity of single or double-membraned Gram-negative organisms. Furthermore, those studies relied on indirect fluorometric observations instead of direct microscopic imaging [12,46]. Treatment of *S. aureus* and *E. coli* with **AMP-016** lead to membrane disruption accompanied by the formation of protruding blebs and holes as visualized by SEM (Figs. 3) and transmission electron microscopy (not shown). The carpet mechanism of membrane disruption is commonly associated with detergent-like antibacterials displaying indiscriminate cell lytic properties and AMPs acting by this mechanism may possess some basic structural requirements [8]. Herein, we have shown that AMPs that disrupt membranes in a detergent like fashion are sensitive to subtle structural modifications. Additionally, the membrane damage in MRSA JE2 and *E coli* K12 was also confirmed by a PI uptake assay and by flow cytometry experiments, showing an increase in the fluorescent intensity of PI after treatment with **AMP-016**.

3.4. In vitro serum stability studies

AMPs have found limited use due to their susceptibility to metabolic enzymes in serum and the liver. Accordingly, some of the **Cit 1.1** analogues were tested for serum stability. **AMP-002** was the most serum-stable peptide of the tested AMPs with about 80% of the peptide remaining after 2 h. of incubation. This was expected because peptides can be degraded starting from the *N*-terminus by exopeptidases [49]. Thus, an alkylated *N*-terminus may be a successful strategy for enhancing AMP stability [30], which may explain the two-fold increase in serum half-life for **AMP-002** compared to **Cit 1.1**. **AMP-006** was also more stable in serum compared to **Cit 1.1,** with approximately 60% of the peptide remaining after a 2-hr. incubation in serum. **AMP-006** had Lys7 and Lys8 substituted by Orn residues. The presence of this unnatural amino acid may prevent recognition by LysC and LysN endopeptidases [50]. *N*-terminus modification and substitution with unnatural amino acids may enhance AMP plasma stability and bioavailability [51], but retaining bioactivity is still paramount. The data suggests alkylation of the *N*-terminus is an interesting strategy to enhance the stability of Cit 1.1 analogues.

3.5. Cytotoxicity

For therapeutic use, AMPs should display good selectivity for bacterial cells over mammalian cells. The active peptides, **AMP-016** and **AMP-017** showed both IC_{50} and HC_{50} values higher than their MICs and displayed minimal hemolytic activity against human red blood cells. We theorized that AMPs should possess a greater affinity for negatively charged bacterial membranes compared to zwitterionic mammalian cell membranes. In fact, prior studies have suggested that AMPs exhibit a higher affinity to bacteria compared to mammalian cells because of their distinct membrane characteristics [7,47,52]. For example, the transmembrane potential is more negative in bacteria cells, which suggest an increase affinity or sensitivity of bacteria cells for cationic antimicrobial peptides [7].

4. Conclusion

We have shown that AMP-membrane interactions impact antimicrobial activity. Rationally designed **Cit 1.1** analogues were used to develop SAR and to elucidate previously unknown interactions responsible for membrane disruption and antibacterial activity. Our insights regarding **Cit 1.1** structural features essential for activity are summarized in Fig. 6. Hydrogen bond donors with a basic pKa at the *N*-terminus were found to be indispensable for antibacterial activity. Ablation of either the hydrogen bond donors or the positive charge resulted in inactivity; suggesting a complementary effect between hydrogen bonding and electrostatic interactions in disrupting membranes. Also, sufficient projections of the side chain amine groups were shown to be essential for membrane disruption. **AMP-016** and **AMP-017** are highly potent **Cit 1.1** analogues with a 2- to 8-fold increase in antimicrobial activity against MRSA. Both analogues have a Trp residue that replaces the native Phe. Thus, the improved activity may be due to an increase in the bulk of the hydrophobic anchor and an improved electrostatic interaction with the negatively-charged membrane. The W3F modification also made **Cit 1.1** analogues active against fungi. NMR studies revealed the propensity of AMPs to form head-to-tail helical-dimers on the surface of anionic membranes and bacterial surfaces. NMR spectroscopy exposed a positive correlation between AMP helicity and antibacterial activity, where *N*-terminal acetylation increased the α-helical structure of the peptides in the absence of a membrane and, correspondingly, lead to a decrease in antibacterial activity. These experiments provide further support for the carpet model of membrane disruption, which was subsequently confirmed by electron microscopy in both Gram-positive and Gram-negative bacteria. The results presented herein provide the critical foundation for further evolving **Cit 1.1** analogues into novel broad-spectrum antibiotics for the treatment of drug-resistant bacterial infections.

5. Experimental section

5.1. Peptide synthesis and purification

AMPs were synthesized using solid phase peptide synthesis (SPPS) on a Focus XC automated peptide synthesizer (AAPPTec, Louisville, KY) on a 0.25 mmol scale. All peptides were synthesized using Fmoc-Rink Amide AM resin support (AAPPTec, Louisville, KY). The resin was wetted in dichloromechane (DCM) for 30 min. to promote swelling. The Fmoc- group was then deprotected twice using 20% 4-methyl piperidine in dimethyl formamide (DMF) (10 mL). The resin was thoroughly washed twice for 10 min. using a 15 mL 1:1 mixture of DCM and DMF. The desired amino acids were then added to obtain a predetermined sequence in the peptide synthesizer. Molecular weight of the AMPs was confirmed by MALDI using a 4800 MALDI TOF/TOF analyzer (SCIEX, Ontario, Canada). The AMPs were purified using a preparative high-performance liquid chromatography (HPLC) using a water (0.1% trifluoroacetic acid (TFA)) and acetonitrile (0.1% TFA) gradient on an HPLC system (Agilent, Santa Clara, CA) with a reverse phase column (Kinetex5 u XB-C18 100 A, 150 × 30.0 mm column). Each AMP was confirmed to be > 95% pure. The relative hydrophobicity of the AMPs was determined by simultaneously measuring retention times with the analytical HPLC system described above.

Special peptide modifications were done on resin and described as follows:

AMP-002 was synthesized by coupling a Sar instead of glycine following the procedure described above.

AMP-003 was acetylated by shaking the complete peptide loaded resin in 1 mL acetic anhydride dissolved in 5 mL (DCM:DMF = 1:1) for 6 h at ambient temperature.

AMP-004 was synthesized by methylating the Fmoc-deprotected *N*-terminus by adding 4 mL methyl iodide and 200 μL triethylamine to the resin in 10 mL DCM and then gently heating at 45 ^{O}C for 5 days.

AMP-005 was synthesized by substituting the glycine residue with bromoacetic acid using the same coupling procedure as described above. The bromine was then displaced with 10 mL hydrazine hydrate

by reacting it on the resin for 24 h.

AMP-010 was synthesized by first making **GLFDVIK(Alloc)K (Alloc)VASVIGGL** on the resin. The *N*-terminus Fmoc was deprotected following the procedure described above. The side chain Alloc was deprotected on resin by treatment with 0.35 eq of $Pd(PPh_3)_4$ and 20 eq of Phenyl silane in DCM for 45 min. Methylation of the free primary amines was achieved by adding 4 mL methyl iodide and 200 μL triethylamine to the resin in 10 mL DCM and then gently heating at 45 °C for 5 days.

AMP-011 was synthesized by first making **Fmoc-GLFDVIK(Alloc)K (Alloc)VASVIGGL** on the resin. The side chain Alloc was deprotected on the resin by treatment with 0.35 eq $Pd(PPh_3)_4$ and 20 eq Phenyl silane in 10 mL DCM for 45 min. Methylation of the free primary amines were achieved by adding 4 mL methyl iodide and 200 μL triethylamine to the resin in 10 mL DCM and then gently heating at 45 °C for 5 days. Finally, the Fmoc- group was deprotected following the procedure described above.

5.2. Minimum inhibitory concentration assay (MIC)

MICs for **Cit 1.1** and the **Cit 1.1** analogues were measured using the following bacterial strains: *S. aureus* JE2 and *E. coli* K12. The MICs was determined using the broth microdilution method as previously described [52]. A stock solution of each peptide was prepared in milliQ water and then serial 2-fold dilutions were made in Difco™ Muller Hinton Broth (MHB) (BD Diagnostics, Becton Drive, NJ) in Cellstar 96-well microtiter plates (Greiner Bio-One, Kremsmünster, Austria). Bacterial cultures were prepared using the direct colony suspension method to 1.5×10^8 colony forming unit (CFU)/mL (0.5 McFarland) and diluted from 2 mL into 40 mL of MHB. Each well was inoculated with 10 μL of bacterial cultures. Plates were statically incubated at 37 °C for 24 h. MIC values correspond to the lowest AMP concentration that yielded no observable bacterial growth based on analysis with the unaided eye or a microplate reader. The optical density (O.D.) value at 600 nm was recorded using an AccuSkan, MultiSkan FC (Thermo Fisher, Waltham, MA). Vancomycin (Sigma, St. Louis, MO) and gentamicin (Alfa Aesar, Ward Hill, MA) were used as positive controls. Blank media was used as a negative control. All assays were performed in triplicates using three independent measurements. All assays were performed in triplicates using three independent measurements.

5.3. NMR structure determination

Unlabeled **Cit 1.1** and the **Cit 1.1** analogues samples were prepared similarly to previous studies [15]. Briefly, 2 mM of **Cit 1.1**, **AMP-003**, or **AMP-016** were dissolved in 90% H_2O and 10% D_2O with 120 mM of SDS-d_{25} (Cambridge Isotope, Ewksbury, MA), 50 mM trimethylsilylpropanoic acid (TMSP), and PBS buffer at pH 7 (uncorrected). NMR experiments were collected at 25 °C on a 700 MHz Avance III spectrometer (Bruker, Billerica, MA) equipped with a 5 mm QCI-P probe with cryogenically cooled carbon and proton channels. ^{1}H chemical shift and NOE assignments were accomplished with TOCSY, DQF-COSY, and NOESY experiments with chemical shifts referenced to TMSP. NMR spectra were collected with 32 transients and 512 points in the indirect dimension. NOESY spectra were collected with mixing times of 100 ms and 200 ms. Inter-strand NOEs were identified using a 3D X-filtered experiment with a mixing time of 120 ms and a 50/50 mixture of unlabeled peptide and a peptide uniformly ^{13}C, ^{15}N labeled at Leu2 [53]. Initial models of the AMPs were generated from Hα chemical shifts using the CS-Rosetta webserver at the BMRB [54]. Structural refinement was carried out with XPLOR-NIH with dimer symmetry enforced [55]. The three AMP dimer structures were determined with 536 to 622 intramolecular NOE restraints, and 16 intermolecular (peptide-peptide) NOE restraints. A total of 400 models were calculated per AMP and the lowest 20 energy structures were subsequently subjected to water refinement in XPLOR-NIH. Validation of the AMP ensembles was done using the Protein Structure Validation Software (PSVS, http://psvs-1_5-dev.nesg.org/) suite from the Northeast Structural Genomics Consortium (NESG) [56].

5.4. One-dimensional NMR temperature titration

The unlabeled NMR **Cit 1.1**, **AMP-003**, or **AMP-016** samples used for structure determination were also subjected to a temperature titration to monitor structure stability. 1D ^{1}H NMR spectra were recorded at temperatures of 25, 30, 40, 50, 60, and 70 °C with 64 transients, 131k data points, and a spectral width of 12.87 ppm. Between each experiment, the samples were allowed to rest at the target temperature for 5 min before data collection. Following the titration, the 25 °C spectrum was recollected to ensure that the sample did not undergo irreversible degradation upon heating.

5.5. Paramagnetic relaxation enhancement titration

The unlabeled NMR **Cit 1.1**, **AMP-003**, or **AMP-016** samples used for structure determination were also used to observe the effects of a diethylenetriaminepentaacetic acid gadolinium (III) dihydrogen salt hydrate (Gd-DTPA) titration. Gd-DTPA was titrated into the samples to concentrations of 0, 2, 4, 8, 16, and 24 mM. 1D ^{1}H NMR spectra were recorded with 128 transients, 64k data points, and a spectral width of 12.87 ppm. Effects resulting from sample dilution were accounted for by normalizing peak intensities to TMSP.

5.6. Scanning electron microscopy (SEM)

E. coli K12 and *S. aureus* JE2 were cultured in MHB and incubated at 37 °C. The resultant mid-log phase cultures were diluted to a final concentration of 1.5×10^8 CFU/ml (0.5 McFarland). The bacteria cells were treated with **Cit 1.1** or a **Cit 1.1** analogue at 2X the MIC value and incubated for 1 h at 37 °C. A control was prepared by adding only media. After AMP treatment, the cells were immediately washed thrice with HyClone™ Dulbecco's PBS solution (GE Healthcare Life Science, Marlborough, MA) and fixed with 2.0% (v/v) glutaraldehyde [57]. The bacterial suspension was then placed on 0.1% Poly-L Lysine coated glass slide and allowed to adhere for 30 min. The slides were washed thrice with PBS to remove excess fixative. Samples were post-fixed in a 1% solution of OsO_4 for 30 min. to facilitate conductivity. The samples were then dehydrated in a graded ethanol series (50, 70, 90, 95, and 100%). Ethanol was removed by washing the slides thrice with hexamethyldisilazane (HMDS). HMDS was allowed to evaporate overnight to dryness. The glass slides were attached to aluminum SEM stubs with double-sided carbon tape. Silver paste was applied to enhance conductivity, which was allowed to dry overnight. Samples were then coated with approximately 50 nm gold-palladium alloy in a Hummer VI Sputter Coater (Anatech, Battle Creek, MI) and imaged at 30 kV in a Quanta 200 SEM (FEI, Hillsboro, OR) operating in high vacuum mode.

5.7. Propidium iodide (PI) uptake

The PI uptake assay was performed according to Shireen et al [58]. *S. aureus* JE2 and *E. coli* K12 cells were grown in BHI broth to the mid logarithmic-phase and the bacterial cells were harvested by centrifugation at 5000 rpm for 5 min and washed once with PBS buffer. Cells were diluted to 10^7 cfu/ml using PBS buffer. AMPs were added to each well at twice the MIC. Similarly, 10 μg/mL of PI was also added to each well. Polymyxin B was used as a reference drug and cells with no AMP treatment were used as a control. PI fluorescence was measured at 37 °C and at 20 min intervals for a total duration of 120 min. The PI fluorescence was measured using a spectrofluorometer with excitation and emission wavelengths set at 544 nm and 620 nm, respectively.

5.8. In vitro human serum stability studies

Cit 1.1 and **Cit 1.1** analogues were incubated in human serum for 2 h in a shaking water bath (90 rpm) at 37 °C. Peptide content in the reaction mixture was below 0.5% (v/v). At select time intervals of 0, 30, 45, 60 and 120 min, 100 µL of the serum-AMP mixture was extracted and quenched with 400 µL of methanol containing oxibendazole as an internal standard. Samples were mixed and centrifuged at 17,950 × *g* for 15 min. at 4 °C. 100 µL of the supernatant was removed for analysis. Stability results were expressed as a percentage of AMP remaining in the serum as a function of time. AMP stability was represented as the percentage of the AMP remaining relative to the first time-point (0 min; 100% AMP). All experiments were performed in triplicate.

A LabSolutions LCMS Ver.5.6 controlled UPLC and MS system consisting of a Shimadzu LC–MS/MS 8060 equipped with a DUIS source, two pumps (LC-30 AD), a column oven (CTO-30AS) and an auto-sampler (SIL-30AC) were used to quantitate AMPs in human serum. The MS/MS system was operated at unit resolution in the multiple reaction monitoring (MRM) mode using the precursor ion to product ion combinations of: (i) 538.92 to 86.20 *m/z*, (ii) 543.60–86.20 *m/z*, (iii) 557.60–86.25 *m/z*, (iv) 529.60–86.25 *m/z*, (v) 548.25 to143.20 *m/z*, and (vi) 551.95 to 86.20 *m/z* for **Cit 1.1**, **AMP-002**, **AMP-006**, **AMP-012, AMP-013** and **AMP-016**, respectively. All of the AMPs were triply charged (m + 3). Mass detection ocoored in the positive ionization mode with the following parameters: nebulizer gas: 2.0 L/min; heating gas: 10 L/min; drying gas: 10 L/min; interface temperature: 375 °C; desolvation line temperature: 250 °C; and heat block temperature: 400 °C.

Acceptable resolution and peak shape were achieved for the AMPs on a BEH C18 (1.7 µg/mL, 2.1 × 100 mm, Waters, Milford, MA) column protected with a C_{18} guard column (Phenomenex, Torrance, CA). The mobile phase consisted of 0.1% formic acid in water (mobile phase A) and methanol (MeOH) (mobile phase B) at total flow rate of 0.25 mL/min. Chromatographic separation was achieved using an 8-minute gradient elution. The initial mobile phase composition was 35% B, which was increased linearly to 95% B over 6 min. The mobile phase was then held constant at 95% B for 1.0 min and returned to the initial condition in 0.5 min followed by a 1 min equilibration. The sample injection volume was 5 µL. Calibration curves were established for each analyte using the peak area ratio (analyte/IS) and known concentration. Each calibration curve consisted of a blank sample, a zero blank (blank and IS), and eight non-zero concentrations. All analytes were extracted from the respective matrix by simple protein precipitation extraction using methanol spiked with the IS. The method was linear over the range from 1 to 1000 ng/mL for all analytes. The acceptance criteria for each back calculated standard concentration was ± 15% standard deviation (SD) from the nominal value except at LLOQ, which was set at ± 20%.

Declaration of Competing Interest

The authors declare no competing financial interest.

Acknowledgements

This work was funded by UNMC-startup funds (MC-S), National Institute of Health-NIGMS, Nebraska Center for Molecular Target Discovery and Development (1P20GM121316-01A1, PI: Robert Lewis, Project Leader, MC-S), and by the USA Department of Defense-Peer Reviewed Medical Research Program 2017 (W81XWH-18-1-0113, MC-S). This work was supported by funding from the Redox Biology Center (P30 GM103335, NIGMS, RP) and the Nebraska Center for Integrated Biomolecular Communication (P20 GM113126, NIGMS, RP). The research was performed in facilities renovated with support from the N.I.H. (RR015468-01). Some antimicrobial tests (as detailed in the SI) were performed by The Community for Antimicrobial Drug Discovery (CO-ADD), funded by the Wellcome Trust (UK) and The University of Queensland (Australia). The authors thank Dr. Andrew Dudley, Tom Bargar, and Nicholas Conoan (UNMC-Electron Microscopy Core Facility, EMCF) and Samantha Wall (UNMC-Flow Cytometry Research Facility, FCRF) for technical assistance. The EMCF and FCRF are supported by the Nebraska Research Initiative (NRI), the University of Nebraska Foundation, and the UNMC-Office of the Vice Chancellor for Research. FCRF is also supported by The Fred and Pamela Buffett Cancer Center's through the NCI.

Appendix A. Supplementary data

Supplementary material related to this article can be found, in the online version, at doi:https://doi.org/10.1016/j.peptides.2019.170119.

References

[1] D.M. Livermore, Bacterial resistance: origins, epidemiology, and impact, Clin. Infect. Dis. 36 (Suppl. 1) (2003) S11–23.
[2] J. O'Neil, Review on antimicrobial resistance, Antimicrobial Resistance: Tackling a Crisis for the Health and Wealth of Nations 2014, (2014).
[3] C. Walsh, Molecular mechanisms that confer antibacterial drug resistance, Nature 406 (6797) (2000) 775–781.
[4] F.C. Tenover, Mechanisms of antimicrobial resistance in bacteria, Am. J. Infect. Control 34 (5) (2006) S3–S10.
[5] D.L. Paterson, Resistance in gram-negative bacteria: enterobacteriaceae, Am. J. Med. 119 (6) (2006) S20–S28.
[6] J. Lin, K. Nishino, M.C. Roberts, M. Tolmasky, R.I. Aminov, L. Zhang, Mechanisms of antibiotic resistance, Front. Microbiol. 6 (2015).
[7] M.R. Yeaman, N.Y. Yount, Mechanisms of antimicrobial peptide action and resistance, Pharmacol. Rev. 55 (1) (2003) 27–55.
[8] Y. Shai, Mode of action of membrane active antimicrobial peptides, Pept. Sci. 66 (4) (2002) 236–248.
[9] K.A. Brogden, Antimicrobial peptides: pore formers or metabolic inhibitors in bacteria? Nat. Rev. Microbiol. 3 (3) (2005) 238–250.
[10] M.A. Sani, F. Separovic, How membrane-active peptides get into lipid membranes, Acc. Chem. Res. 49 (6) (2016) 1130–1138.
[11] M. Zasloff, Antimicrobial peptides of multicellular organisms, Nature 415 (6870) (2002) 389.
[12] M.P. Boland, F. Separovic, Membrane interactions of antimicrobial peptides from Australian tree frogs, Biochim. Biophys. Acta Biomembr. 1758 (9) (2006) 1178–1183.
[13] M. Jaskiewicz, M. Orlowska, G. Olizarowicz, D. Migon, D. Grzywacz, W. Kamysz, Rapid screening of antimicrobial synthetic peptides, Int. J. Pept. Res. Ther. 22 (2) (2016) 155–161.
[14] W. Kamysz, P. Nadolski, A. Kedzia, O. Cirioni, F. Barchiesi, A. Giacometti, G. Scalise, J. Lukasiak, M. Okroj, In vitro activity of synthetic antimicrobial peptides against Candida, Pol. J. Microbiol. 55 (4) (2006) 303–307.
[15] E. Sikorska, K. Greber, S. Rodziewicz-Motowidlo, L. Szultka, J. Lukasiak, W. Kamysz, Synthesis and antimicrobial activity of truncated fragments and analogs of citropin 1.1: the solution structure of the SDS micelle-bound citropin-like peptides, J. Struct. Biol. 168 (2) (2009) 250–258.
[16] J. Doyle, C.S. Brinkworth, K.L. Wegener, J.A. Carver, L.E. Llewellyn, I.N. Olver, J.H. Bowie, P.A. Wabnitz, M.J. Tyler, nNOS inhibition, antimicrobial and anticancer activity of the amphibian skin peptide, citropin 1.1 and synthetic modifications, Eur. J. Biochem. 270 (6) (2003) 1141–1153.
[17] A.N. Calabrese, K. Markulic, I.F. Musgrave, H. Guo, L. Zhang, J.H. Bowie, Structural and activity changes in three bioactive anuran peptides when Asp is replaced by isoAsp, Peptides 38 (2) (2012) 427–436.
[18] A. Giacometti, O. Cirioni, W. Kamysz, C. Silvestri, M.S. Del Prete, A. Licci, G. D'Amato, J. Łukasiak, G. Scalise, In vitro activity and killing effect of citropin 1.1 against gram-positive pathogens causing skin and soft tissue infections, Antimicrob. Agents Chemother. 49 (6) (2005) 2507–2509.
[19] B. Chia, Y. Gong, J.H. Bowie, J. Zuegg, M.A. Cooper, Membrane binding and perturbation studies of the antimicrobial peptides caerin, citropin, and maculatin, Biopolymers 96 (2) (2011) 147–157.
[20] E. Strandberg, A.S. Ulrich, NMR methods for studying membrane-active antimicrobial peptides, concepts, Magn. Reson. Part A 23A (2) (2004) 89–120.
[21] A. Bax, Two-dimensional NMR and protein structure, Annu. Rev. Biochem. 58 (1) (1989) 223–256.
[22] D.S. Wishart, C.G. Bigam, A. Holm, R.S. Hodges, B.D. Sykes, 1H, 13C and 15N random coil NMR chemical shifts of the commom amino acids. I. Investigations of nearest-neighbor effects, J. Biomol. NMR 5 (1995) 67–81.
[23] S. Schwarzinger, G.J.A. Kroon, T.R. Foss, J. Chung, P.E. Wright, H.J. Dyson, Sequence-dependent correction of random coil NMR chemical shifts, J. Am. Chem. Soc. 123 (2001) 2970–2978.
[24] R.A. Laskowski, M.W. MacArthur, D.S. Moss, J.M. Thornton, PROCHECK: a program to check the stereochemical quality of protein structures, J. Appl. Cryst. 26 (2) (1993) 283–291.

[25] G.M. Clore, J. Iwahara, Theory, practice, and applications of paramagnetic relaxation enhancement for the characterization of transient low-population states of biological macromolecules and their complexes, Chem. Rev. 109 (2009) 4108–4139.
[26] L. Di, Strategic approaches to optimizing peptide ADME properties, AAPS J. 17 (1) (2014) 134–143.
[27] E.M. Spencer, Isoelectric heterogeneity of bovine plasma albumin, J. Biol. Chem. 246 (1) (1971) 201–208.
[28] C.Z. Chen, N.C. Beck-Tan, P. Dhurjati, T.K. van Dyk, R.A. LaRossa, S.L. Cooper, Quaternary ammonium functionalized poly (propylene imine) dendrimers as effective antimicrobials: structure-activity studies, Biomacromolecules 1 (3) (2000) 473–480.
[29] T. Thorsteinsson, M. Másson, K.G. Kristinsson, M.A. Hjálmarsdóttir, H. Hilmarsson, T. Loftsson, Soft antimicrobial agents: synthesis and activity of labile environmentally friendly long chain quaternary ammonium compounds, J. Med. Chem. 46 (19) (2003) 4173–4181.
[30] L. Gentilucci, R. De Marco, L. Cerisoli, Chemical modifications designed to improve peptide stability: incorporation of non-natural amino acids, pseudo-peptide bonds, and cyclization, Curr. Pharm. Des. 16 (28) (2010) 3185–3203.
[31] E. McCleskey, W. Almers, The Ca channel in skeletal muscle is a large pore, Proc. Natl. Acad. Sci. 82 (20) (1985) 7149–7153.
[32] D.L. Nelson, A.L. Lehninger, M.M. Cox, Lehninger Principles of Biochemistry, Macmillan, 2008.
[33] A. Bagno, E. Menna, E. Mezzina, G. Scorrano, D. Spinelli, Site of protonation of alkyl- and arylhydrazines probed by 14N, 15N, and 13C NMR relaxation and quantum chemical calculations, J. Phys. Chem. A 102 (17) (1998) 2888–2892.
[34] D.I. Chan, E.J. Prenner, H.J. Vogel, Tryptophan-and arginine-rich antimicrobial peptides: structures and mechanisms of action, Biochim. Biophys. Acta 1758 (9) (2006) 1184–1202.
[35] L. Jin, X. Bai, N. Luan, H. Yao, Z. Zhang, W. Liu, Y. Chen, X. Yan, M. Rong, R. Lai, A designed tryptophan-and Lysine/Arginine-Rich antimicrobial peptide with therapeutic potential for clinical antibiotic-resistant Candida albicans vaginitis, J. Med. Chem. 59 (5) (2016) 1791–1799.
[36] J. Svenson, R. Karstad, G.E. Flaten, B.-O. Brandsdal, M. Brandl, J.S. Svendsen, Altered activity and physicochemical properties of short cationic antimicrobial peptides by incorporation of arginine analogues, Mol. Pharm. 6 (3) (2009) 996–1005.
[37] K.E.S. Locock, T.D. Michl, J.D.P. Valentin, K. Vasilev, J.D. Hayball, Y. Qu, A. Traven, H.J. Griesser, L. Meagher, M. Haeussler, Guanylated polymethacrylates: a class of potent antimicrobial polymers with low hemolytic activity, Biomacromolecules 14 (11) (2013) 4021–4031.
[38] D.J. Mitchell, L. Steinman, D.T. Kim, C.G. Fathman, J.B. Rothbard, Polyarginine enters cells more efficiently than other polycationic homopolymers, J. Pept. Res. 56 (5) (2000) 318–325.
[39] I. Nakase, S. Okumura, S. Katayama, H. Hirose, S. Pujals, H. Yamaguchi, S. Arakawa, S. Shimizu, S. Futaki, Transformation of an antimicrobial peptide into a plasma membrane-permeable, mitochondria-targeted peptide via the substitution of lysine with arginine, Chem. Commun. 48 (90) (2012) 11097–11099.
[40] E.E. Ambroggio, F. Separovic, J.H. Bowie, G.D. Fidelio, L.A. Bagatolli, Direct visualization of membrane leakage induced by the antibiotic peptides: maculatin, citropin, and aurein, Biophys. J. 89 (3) (2005) 1874–1881.
[41] M.R.R. de Planque, B.B. Bonev, J.A.A. Demmers, D.V. Greathouse, R.E. Koeppe, F. Separovic, A. Watts, J.A. Killian, Interfacial anchor properties of tryptophan residues in transmembrane peptides can dominate over hydrophobic matching effects in peptide − lipid interactions, Biochemistry 42 (18) (2003) 5341–5348.
[42] B.E. Haug, J.S. Svendsen, The role of tryptophan in the antibacterial activity of a 15-residue bovine lactoferricin peptide, J. Pept. Sci. 7 (4) (2001) 190–196.
[43] Y. Chen, M.T. Guarnieri, A.I. Vasil, M.L. Vasil, C.T. Mant, R.S. Hodges, Role of peptide hydrophobicity in the mechanism of action of alpha-helical antimicrobial peptides, Antimicrob. Agents Chemother. 51 (4) (2007) 1398–1406.
[44] W.-M. Yau, W.C. Wimley, K. Gawrisch, S.H. White, The preference of tryptophan for membrane interfaces, Biochemistry 37 (42) (1998) 14713–14718.
[45] A. Chakrabartty, A.J. Doig, R.L. Baldwin, Helix capping propensities in peptides parallel those in proteins, PNAS 90 (1993) 11332–11336.
[46] T. Salditt, C. Li, A. Spaar, Structure of antimicrobial peptides and lipid membranes probed by interface-sensitive X-ray scattering, Biochim. Biophys. Acta 1758 (9) (2006) 1483–1498.
[47] A. Giuliani, G. Pirri, A. Bozzi, A. Di Giulio, M. Aschi, A. Rinaldi, Antimicrobial peptides: natural templates for synthetic membrane-active compounds, Cell. Mol. Life Sci. 65 (16) (2008) 2450–2460.
[48] J.M. Henderson, A.J. Waring, F. Separovic, K.Y.C. Lee, Antimicrobial peptides share a common interaction driven by membrane line tension reduction, Biophys. J. 111 (10) (2016) 2176–2189.
[49] C.F. Deacon, M.A. Nauck, M. Toft-Nielsen, L. Pridal, B. Willms, J.J. Holst, Both subcutaneously and intravenously administered glucagon-like peptide I are rapidly degraded from the NH2-terminus in type II diabetic patients and in healthy subjects, Diabetes 44 (9) (1995) 1126–1131.
[50] S. Kawabata, E. Davie, A microsomal endopeptidase from liver with substrate specificity for processing proproteins such as the vitamin K-dependent proteins of plasma, J. Biol. Chem. 267 (15) (1992) 10331–10336.
[51] A.K. Marr, W.J. Gooderham, R.E. Hancock, Antibacterial peptides for therapeutic use: obstacles and realistic outlook, Curr. Opin. Pharmacol. 6 (5) (2006) 468–472.
[52] A.L. Leber, Clinical Microbiology Procedures Handbook, (2004).
[53] A.L. Breeze, Isotope-filtered NMR methods for the study of biomolecular structure and interactions, Prog. Nucl. Magn. Reson. Spectrosc. 36 (1999) 323–372.
[54] Y. Shen, O. Lange, F. Delaglio, P. Rossi, J.M. Aramini, G. Liu, A. Eletsky, Y. Wu, K.K. Singarapu, A. Lemak, A. Ignatchenko, C.H. Arrowsmith, T. Szyperski, G.T. Montelione, D. Baker, A. Bax, Consistent blind protein structure generation from NMR chemical shift data, PNAS 105 (12) (2008) 4685–4690.
[55] C.D. Schwieters, J.J. Kuszewski, G.M. Clore, Using Xplor-NIH for NMR molecular structure determination, J. Magn. Reson. 48 (2006) 47–62.
[56] A. Bhattacharya, R. Tejero, G.T. Montelione, Evaluating protein structures determined by structural genomics consortia tools for structure quality evaluation, Proteins 66 (2007) 778–795.
[57] M. Hartmann, M. Berditsch, J. Hawecker, M.F. Ardakani, D. Gerthsen, A.S. Ulrich, Damage of the bacterial cell envelope by antimicrobial peptides gramicidin S and PGLa as revealed by transmission and scanning electron microscopy, Antimicrob. Agents Chemother. 54 (8) (2010) 3132–3142.
[58] T. Shireen, S. Venugopal, D. Ghosh, R. Gadepalli, B. Dhawan, K. Mukhopadhyay, In vitro antimicrobial activity of alpha-melanocyte stimulating hormone against major human pathogen *Staphylococcus aureus*, Peptides 30 (9) (2009) 1627–1635.